AIP | Chaos
An Interdisciplinary Journal of Nonlinear Science

Variability of spatio-temporal patterns in non-homogeneous rings of spiking neurons

Serhiy Yanchuk, Przemyslaw Perlikowski, Oleksandr V. Popovych, and Peter A. Tass

Citation: Chaos **21**, 047511 (2011); doi: 10.1063/1.3665200
View online: http://dx.doi.org/10.1063/1.3665200
View Table of Contents: http://chaos.aip.org/resource/1/CHAOEH/v21/i4
Published by the American Institute of Physics.

Variability of spatio-temporal patterns in non-homogeneous rings of spiking neurons

Serhiy Yanchuk,[1] Przemyslaw Perlikowski,[2] Oleksandr V. Popovych,[3] and Peter A. Tass[3,4]
[1]*Institute of Mathematics, Humboldt University of Berlin, 10099 Berlin, Germany*
[2]*Division of Dynamics, Technical University of Lodz, 90-924 Lodz, Poland*
[3]*Institute of Neurosciences and Medicine - Neuromodulation (INM-7), Research Center Jülich, 52425 Jülich, Germany*
[4]*Department of Stereotaxic and Functional Neurosurgery, University Hospital, 50924 Cologne, Germany*

(Received 30 August 2011; accepted 11 November 2011; published online 29 December 2011)

We show that a ring of unidirectionally delay-coupled spiking neurons may possess a multitude of stable spiking patterns and provide a constructive algorithm for generating a desired spiking pattern. More specifically, for a given time-periodic pattern, in which each neuron fires once within the pattern period at a predefined time moment, we provide the coupling delays and/or coupling strengths leading to this particular pattern. The considered homogeneous networks demonstrate a great multistability of various travelling time- and space-periodic waves which can propagate either along the direction of coupling or in opposite direction. Such a multistability significantly enhances the variability of possible spatio-temporal patterns and potentially increases the coding capability of oscillatory neuronal loops. We illustrate our results using FitzHugh-Nagumo neurons interacting via excitatory chemical synapses as well as limit-cycle oscillators. © *2011 American Institute of Physics*. [doi:10.1063/1.3665200]

Feed-forward loops of coupled neurons are generic components of nervous systems. Describing the dynamics in such loops, especially, the emergence of stable spiking patterns is crucial for understanding neuronal information processing and storage. It has been shown that unidirectionally coupled loops of neurons may have amazing dynamical properties. For instance, stable travelling waves may emerge that travel not only in the direction of the coupling but also in opposite direction. In this paper, we present a concept that goes beyond the phenomenon of travelling waves. In fact, we show that a great variety of complex time-periodic spiking patterns, in which each neuron fires once within the pattern period, can be generated by a feed-forward loop. Moreover, we provide a recipe that enables to select the pattern of coupling delays and/or coupling strengths leading to a desired spiking pattern. Since the nervous system is able to tune both synaptic weights and communication delays, it is able to generate, store, and retrieve a multitude of stable spiking patterns in such a generic neuronal module. Accordingly, this may contribute to the striking coding capability of nervous systems.

I. INTRODUCTION

Delayed interactions can cause time-shifts between signals. This has been shown experimentally for two lasers coupled with a time delay.[1] However, in-phase synchronization is still possible in many delay-coupled networks. In particular, for in-phase synchronization observed for distant intra-cortical neuronal populations, a network motif has been suggested, where a neuronal population in the thalamus can serve as a mediator.[2] Besides in-phase synchronization, the emergence of more complicated spatio-temporal structures and its control in coupled systems became a topic of increasing interest.[3,4] Spatio-temporal patterns of this kind are particularly important in the framework of the temporal coding hypothesis, where the information of a neural spike train generated by a single neuron or by a neural population is hypothesized to be carried by the timing of the action potentials.[5,6] Hence, the variety of spatio-temporal firing patterns appearing in neuronal ensembles[7–9] play an important role for neural coding.

The modulation of signal propagation delays, coupling topology, and synaptic weights within and between neural clusters can affect the formation of such patterns.[6,10,11] In the brain, the synaptic weights can permanently be adjusted due to the spike timing-dependent plasticity, for review see Ref. 12. Propagation delays also seem to be well-tuned in the brain[13] and can be adapted either by synaptic selection out of a spectrum of many possible delay lines[14,15] or directly by changing length and thickness of dendrites and axons, the extent of myelination of axons, variation of synaptic latencies, etc.[16–18] Accordingly, pathological alterations of the signal conductance can severely impair neural information processing as, for example, in the case of axon demyelination in multiple sclerosis.[19]

In this paper, we show how a variety of spiking patterns may stably appear in an oscillatory neuronal loop by appropriate adjustment of communication delays and synaptic weights. In particular, for any time-periodic spiking pattern, in which each neuron spikes once per the pattern period at an arbitrary given position within the period, we explicitly provide the values of the communication delays leading to such a pattern. We show that not only the inhomogeneity of the communication delays, but also the inhomogeneity of the

synaptic weights as well as their combination can create a great variability of spiking patterns. Moreover, even assuming completely homogeneous couplings and delays, various spiking patterns can be created by altering properties of individual neurons. Our results indicate that such a simple unidirectional ring coupling topology already possesses striking coding capabilities taking into account the inhomogeneities, which may naturally occur in neural systems. Some of the above results have briefly been reported for ensembles of limit-cycle oscillators and Hodgkin-Huxley spiking neurons in our short communication.[20] In this paper, we further extend our investigations of the emergence of spatio-temporal patterns, also, for another neuronal model.

As mentioned above, we consider unidirectionally coupled loops which are generic components in the nervous system, where many neural circuits are organized in feed-forward loops[21,22] as intensively studied, e.g., in the context of pathological neural dynamics[23,24] and deep brain stimulation.[25] Such networks are involved in the generation of stable periodic motor commands by central pattern generators of the nervous system controlling rhythmic locomotion in animals.[26] In studies on the propagation of neural activity along feed-forward chains,[27] traveling waves turned out to be typical solutions.[28] Many theoretical studies are devoted to nonlinear dynamics in rings of coupled systems.[29–43] In particular, the existence and stability of phase-locked patterns and amplitude death states;[37] periodic[39,41,42,44,45] and chaotic travelling waves;[32,46,47] transient oscillations;[48,49] bifurcating periodic orbits[44,45] have been reported. It was shown in Refs. 39, 43, 50 that the transition from stationary to oscillatory behavior in such systems is mediated by a bifurcation scenario, which includes the appearance of multiple periodic orbits with different frequencies and spatial organization.

We note that an internal or external noise, which is inherently present in real neural networks, can also improve the timing precision of the neuronal spiking, as shown by Frank Moss and co-workers[51,52] for the case of deterministically sub-threshold stimuli in an array of noisy Hodgkin-Huxley neurons or in-phase synchronized states of locally coupled nonidentical units of the FitzHugh-Nagumo type driven by additive noise. These results further support the temporal coding hypothesis and underline the importance of studying the emergence mechanisms of complex spatio-temporal firing patterns in neuronal networks.

The structure of the paper is as follows: In Sec. II, we introduce the models of ring-coupled limit cycle (LC) oscillators and FitzHugh-Nagumo (FHN) neurons interacting via excitatory chemical synapses. In Sec. III, we review and extend our previous results on the homogeneous rings of unidirectionally coupled systems. In particular, we describe properties of coexistent multiple travelling waves, e.g., their number, stability, spatial and temporal frequencies, dependencies on the delays, and number of oscillators in the ring. We also show the existence of stable backward travelling waves, which are periodic in time and space and propagate in the direction opposite to the direction of coupling. Further, in Sec. IV, we consider the inhomogeneous rings and demonstrate how various stable spiking patterns can be produced in such a system. In particular, we consider the cases of inhomogeneous communication delays in Sec. IV A, inhomogeneous synaptic weights in Sec. IV B, their combination in Sec. IV C, and essentially non-identical internal parameters of the oscillators for homogeneous couplings and delays in Sec. IV E. Finally, we conclude in Sec. V.

II. THE MODELS

We illustrate our results using two models. The first model is the ring of coupled LC oscillators[53] of the form

$$\dot{z}_j(t) = (\alpha + i\beta)z_j(t) - z_j(t)\left|z_j(t)\right|^2 + K_j z_{j+1}(t-\tau_j), \qquad (1)$$

where z_j, $j=1,\ldots,N$ are complex variables for individual oscillators, α and β are real parameters, $\tau_j > 0$ are time delays of the coupling (see Fig. 1), and K_j are coupling weights. The ring structure implies $z_{N+1} \equiv z_1$. System (1) allows to investigate many properties of periodic solutions analytically, due to the S^1-symmetry with respect to the phase change $z_j \to z_j e^{i\gamma}$. Because of this symmetry, time-periodic solutions bifurcating generically from the homogeneous state $z_1 = \cdots = z_N$ have the simple explicit form $z_j = \rho_j e^{i\omega t + i\varphi_j}$ with some constant amplitudes ρ_j, frequency ω, and phase shifts φ_j. We will use this property in order to obtain analytical characteristics of periodic solutions.

Another, more realistic model is given by a ring of delay-coupled FHN oscillators[54,55] interacting via excitatory chemical synapses

$$\begin{aligned} \dot{v}_j &= v_j - v_j^3/3 - w_j + I_j + K_j(V - v_j)s_{j+1}(t-\tau_j), \\ \dot{w}_j &= 0.08(v_j + 0.7 - 0.8w_j), \\ \dot{s}_j &= 0.5(1-s_j)/(1+\exp(-5(v_j-1))) - 0.6s_j, \\ & \qquad j = 1,2,\ldots,N. \end{aligned} \qquad (2)$$

Here, variable v_j models the membrane potential of a single cell, and I_j is a constant current controlling the spiking dynamics of a neuron. In what follows, we consider I_j being randomly Gaussian distributed around the mean value $\bar{I} = 0.4$ with standard deviation $\sigma = 0.002$. For such values of I_j neurons (2) demonstrate an intrinsically spiking dynamics with spiking frequencies f_j (number of spikes per second) of individual neurons being distributed around the mean frequency $\bar{f} \approx 23.5$ Hz with standard deviation $\sigma_f \approx 0.05$.

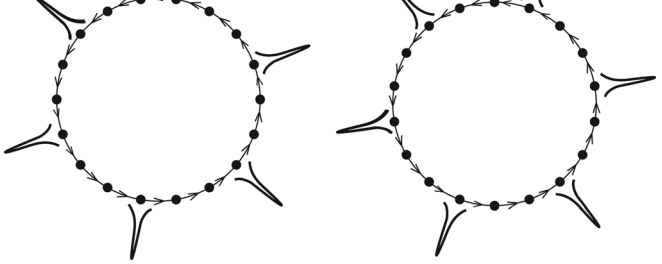

FIG. 1. Coupling scheme and illustration of the spiking fronts, which are propagating along (left figure) and opposite (right figure) to the coupling direction.

The synaptic coupling between the neurons in ensemble (2) is realized via a post-synaptic potential s_j triggered by spikes of neuron j.[56,57] It is modeled in the standard way by an additional equation for $s_j(t)$.[58,59] Parameters K_j define the coupling strength, τ_j are the time delays in coupling, and V is the reversal potential taken as $V=2$ for excitatory coupling. As for the ensemble of LC oscillators (1), we assume that the neurons are unidirectionally coupled in a ring such that $s_{N+1} \equiv s_1$.

The above introduced systems can be written in the general form

$$\dot{x}_j(t) = \mathbf{f}_j(x_j(t), x_{j+1}(t-\tau_j)) \tag{3}$$

with some functions $\mathbf{f}_j$. When the specific details of the systems do not play important role, we will use the representation (3).

III. TRAVELLING FRONTS IN HOMOGENEOUSLY COUPLED SYSTEMS

In this section, we assume that the system is homogeneous, i.e., the coupling strengths $K_j=K$ are identical as well as the interaction delays $\tau_j=\tau$. Although the individual dynamics of oscillators (1) and (2) is described by completely different systems, the topology of the coupling (3) implies that both systems possess travelling wave solutions.[60,61] For coupled LC oscillators, it means that the maxima of the solutions are propagating along the chain periodically with a constant phase-shift between any two neighboring oscillators. In the case of neural systems, this leads to the appearance of firing fronts, which are travelling along the ring. In spite of the unidirectional coupling, the fronts can stably propagate in both directions: along the coupling as well as in the direction opposite to the coupling.

A. Properties of travelling waves in LC coupled systems

Some of the observed stable travelling waves for system (1) are illustrated in Fig. 2. Figure 2a shows a wave with two maxima, which is propagating along the network in the direction opposite to the coupling, i.e., towards the increasing oscillator index j. A similar pattern with one maximum in space is shown in Fig. 2(b), which is obtained in ensemble (1) for the same parameter values, but for different initial condition. Figure 2(c) shows completely synchronized oscillations. Stable patterns, which propagate in the direction along the coupling are shown in Figs. 2(d) and 2(e). All of the illustrated patterns are dynamically stable for the selected parameter values, and, hence, small perturbations as well as small parameter changes do not destroy them.

Periodic travelling waves for ensemble (1) have the following form (for more details, see Ref. 43)

$$z_j(t) = \rho e^{i\omega t + i\varphi_l j}, \quad \text{where} \quad \varphi_l = \frac{2\pi}{N} l. \tag{4}$$

Here, ρ and ω are the amplitude and the oscillation frequency, respectively. φ_l corresponds to a spatial mode with any possible integer l ranging from $-N/2$ to $N/2$. Note that φ_l equals to

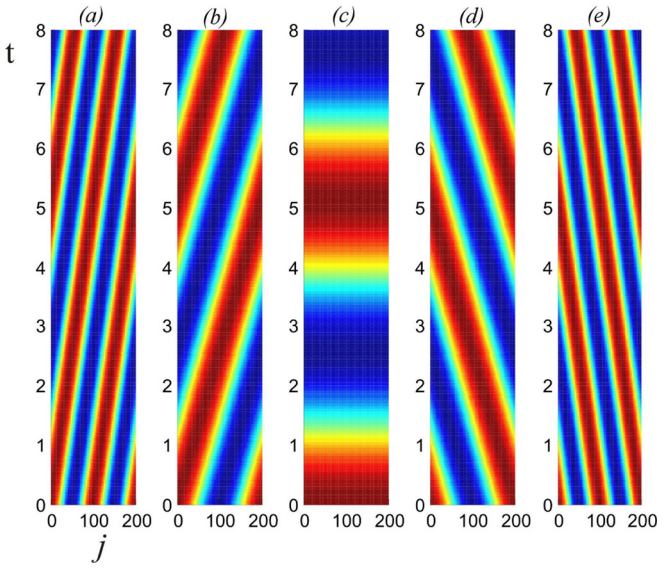

FIG. 2. (Color online) Space-time plots of stable periodic travelling waves in the system of $N=200$ unidirectionally coupled LC oscillators (1) for parameters $\beta=2$, $\alpha=1$, $\tau=10$, and $K=1$. The oscillator index j is shown along the horizontal axes and time t is plotted along the vertical axes. Colors indicate the magnitude of the real part of the trajectory $z_j(t)$ ranging from its maximal value [red] to its minimal value [blue]. In plots (a) and (b), the waves are moving to the right, i.e., against the coupling direction. In the middle plot (c), a completely synchronized regime is illustrated. Plots (d) and (e) depict the travelling waves with (d) one and (e) two maxima which are propagating to the right, i.e., along the direction of the coupling.

the phase shift between the neighboring oscillators. The frequency ω satisfies the following transcendental equation

$$\omega = \beta + K\sin(\varphi_l - \omega\tau). \tag{5}$$

For the given spatial mode φ_l and frequency ω from Eq. (5), the amplitude ρ is given by

$$\rho = \sqrt{\alpha + K\cos(\varphi_l - \omega\tau)}.$$

From Eq. (5), it follows that for any given spatial mode φ_l, multiple frequencies $\omega=\omega_{lk}$ may appear since Eq. (5) admits multiple solutions (here, $k=1,2,\ldots,M(\tau,\ l)$ is the index of different solutions of Eq. (5) for given l and τ), especially for large τ. More specifically, for small τ, a unique frequency ω_l appears for each spatial mode [Figs. 4(a), 4(d)–4(f)]. With increasing τ, more and more frequencies appear for each φ_l [Figs. 4(b), 4(c)]. The number $M(\tau,\ l)$ of different possible frequencies ω_{lk} grows linearly with τ.[62] Such a multistability is typical for systems with large time delay, see, e.g., Refs. 63–65. Figure 3 illustrates this multistability on the example of the in-phase synchronous mode $\varphi_0=0$ by showing spatio-temporal plots of the solutions $z_j(t) = \rho e^{i\omega_{0k}t}$ with $k=1,\ 2,\ 3$.

Figure 4 shows possible oscillation frequencies ω versus spatial modes φ_l. More exactly, the relative number of firing fronts (or maxima of the trajectories $\Re(z_j(t))$ simultaneously travelling along the ring) with respect to the number of oscillators $N_{FF}=l/N$ is plotted along the horizontal axis, which is proportional to φ_l, namely $N_{FF}=\varphi_l/2\pi$. In Figs. 4(a)–4(c), the effect of the time delay is illustrated: with increasing time delay τ, the function ω becomes multivalued and the

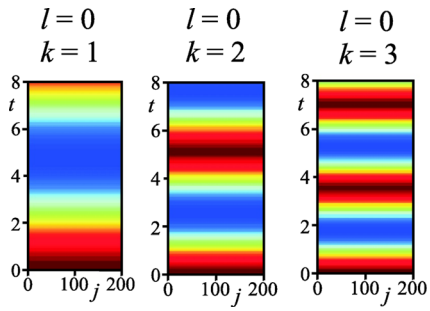

FIG. 3. (Color online) Multistability of the in-phase synchronous regimes with $\varphi_0 = 0$ due to the delay in the coupling. Color depicts the magnitude of the trajectories $\Re(z_j(t))$ as in Fig. 2. The index k enumerates different oscillation frequencies ω_{0k}, which are the solutions of Eq. (5). Similar multistability takes place for other spatial modes φ_l, $l = 1,\ldots,N$. Parameters $\tau = 10$, $\alpha = -0.5$, $\beta = 1$, $N = 200$, and $K = 1$.

multistability increases. Brighter (green online) parts of the curves correspond to stable travelling waves and darker (red online) to unstable. We see that the number of stable and unstable waves are roughly equal for large delays. The impact of the bifurcation parameter α is illustrated in Figs. 4(d)–4(f). The travelling waves start to appear at $\alpha = -|K|$, and for $-|K| < \alpha < 0$, the admissible range of oscillation frequencies is

$$|\omega - \beta| \leq \sqrt{K^2 - \alpha^2}, \tag{6}$$

while for $\alpha > 0$ it reaches its maximum $|\omega - \beta| \leq |K|$. For small τ and α, the range of admissible spatial modes l can also be bounded, see Fig. 4(d). Indeed, as follows from Eqs. (5) and (6), the bounds are

$$|\varphi_l - \beta\tau| \leq \tau\sqrt{K^2 - \alpha^2} + \arccos\left(-\frac{\alpha}{K}\right), \tag{7}$$

for $-K < \alpha < K$ and small τ. With increasing τ or α, the range of admissible spatial modes reaches the maximum $\varphi_j \in [-\pi, \pi]$ according to Eq. (7).

The dependence of the round-trip time of the waves travelling along the ring is illustrated in Figs. 5(a)–5(c). One can observe that the round-trip time continuously depends on N_{FF}. Zero round-trip time corresponds to the homogeneous (completely synchronous) state.

Typical dependence of the intervals ΔT_s between the spikes (maximum values of the trajectories $x_j(t) = \Re(z_j(t))$) of two neighboring oscillators $z_j(t)$ and $z_{j+1}(t)$ on delay time τ is shown in Fig. 5(d). This dependence is shown for some travelling wave with a fixed spatial wavenumber $l = l^* \neq 0$. Although the dependence $\Delta T_s(\tau)$ itself is continuous along the branch, the branch can clearly be decomposed into sub-branches corresponding to different resonances. Each such sub-branch consists of one stable (bright part, green online) and one unstable (dark, red online) part. The stable parts can be well approximated by a linear function of delay indicating the "resonance" character of $\Delta T_s(\tau)$. An interesting property of these sub-branches is that for any travelling wave at time delay τ on one sub-branch, there exists *the same* travelling wave on all other sub-branches for time delays

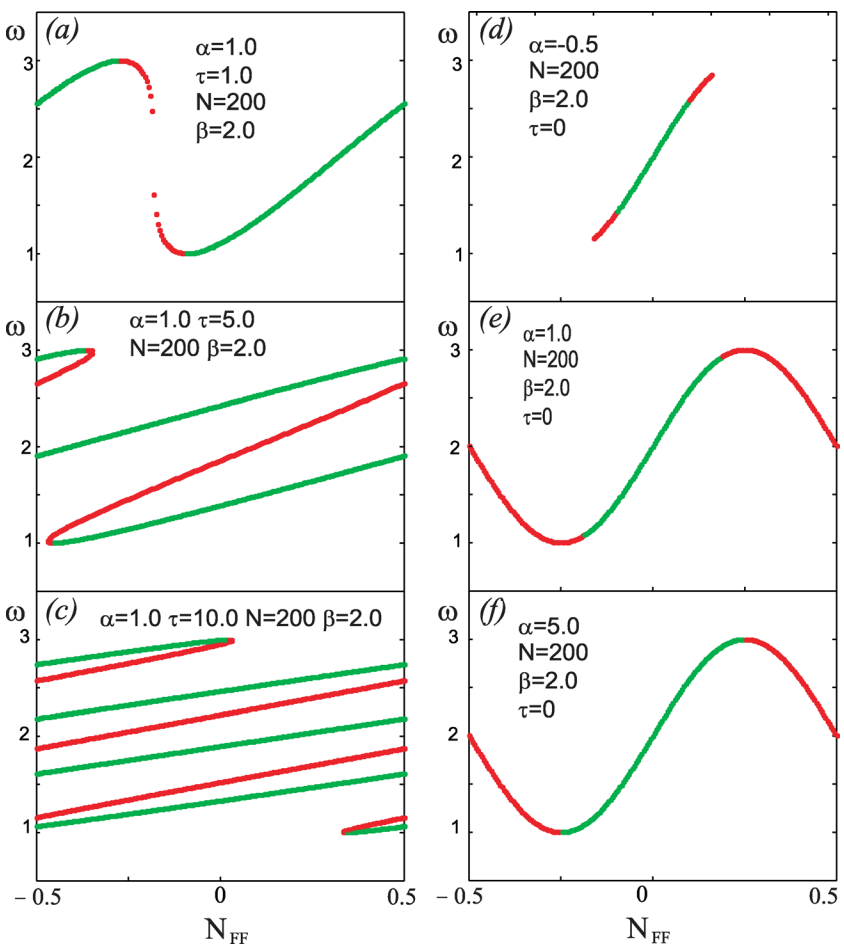

FIG. 4. (Color online) Coexistence of numerous periodic travelling waves and their stability for system (1). Spatial modes are shown along the horizontal axis as $N_{FF} = l/N$, where N_{FF} measures the relative number of the firing fronts travelling along the ring. Oscillation frequencies ω are shown along the vertical axis. The left column illustrates the influence of the delay, where the delay increases from top to bottom. The right column shows the influence of the parameter α. Stable travelling waves are depicted in light gray (green online) and unstable waves in dark gray (red online). Parameters are indicated in the plots.

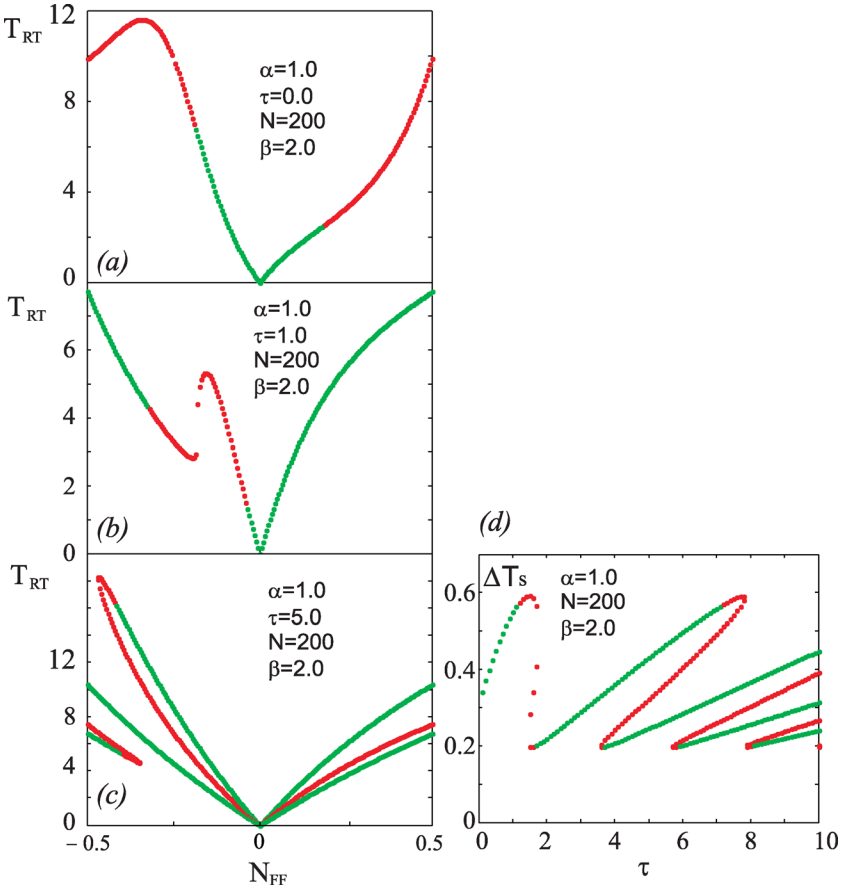

FIG. 5. (Color online) (a)-(c) Round-trip time T_{RT} of the waves travelling along the ring versus the spatial number N_{FF} for the LC ensemble (1). Stable waves are shown in light gray (green online) and unstable waves in dark gray (red online). (d) Inter-spike intervals ΔT_s between two neighboring oscillators versus delay τ for a travelling wave with wavenumber $l \neq 0$. Parameters are indicated in the plots.

$$\tau_m = \tau + m2\pi/\omega(\tau). \tag{8}$$

Here, $\omega(\tau)$ is the frequency of the travelling wave and m is an integer number. Thus, the set of travelling waves on one sub-branch can be mapped by the mapping (8) to any other sub-branch with an appropriate m. This property follows from the fact, that any periodic solution of a system (3) with homogeneous delays $\tau_j = \tau$ with frequency ω is the solution of the same system with time-delay τ_m as well (for more details for general delay differential equations, see Ref. 62). Figure 5(d) also illustrates how the coexistence of multiple travelling waves with the same wavenumber increases as the time delay grows.

B. Perturbations of backward propagating fronts

In the previous sections, we have seen that the unidirectional rings of coupled systems possess periodic regimes of oscillations, in which the maxima of the periodic spikes move against the coupling direction. Such regimes do not contradict to the fact that the information flow in the system is propagating only along the coupling direction. Indeed, any local perturbation in the system will propagate along the coupling direction as illustrated in Fig. 6. We perturb there at time $t = 0$, a small group of oscillators close to $j = 90$. Afterwards, the perturbation is spreading along the coupling direction (here, to the left) and opposite to the spiking front direction.

C. Travelling waves in coupled FitzHugh-Nagumo neurons

The network of FHN neurons (2) unidirectionally coupled in a ring via excitatory chemical synapses also demonstrates a great multistability of travelling waves. Depending on the initial conditions, the neurons can synchronize and fire either simultaneously (in-phase synchronization) or with the time shift $t_j - t_{j+1} \approx Tl/N$ between the neighboring neurons, where T is the period of oscillations. In the latter

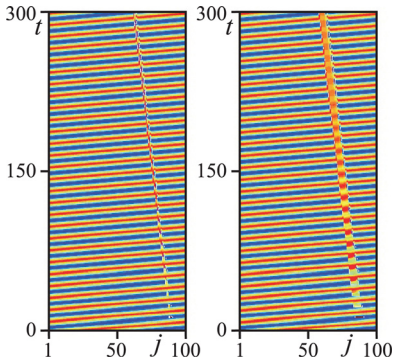

FIG. 6. (Color online) A stable backward propagating wave is locally perturbed. The perturbation is propagating along the coupling direction (to the left) and opposite to the propagation of maxima. (a) Oscillators 80–83 are perturbed. (b) Oscillators 80–86 are perturbed. The amplitude of the travelling waves is ≈ 1.4, while the perturbation amplitude is $\bar{z}_j = 2.0 + i2.0$. Other parameters: $N = 100$, $\tau = 10$, $\alpha = 1.0$, and $\beta = 0$.

case, l firing fronts propagate along the network either in the direction of coupling or in opposite direction. Although an isolated FHN neuron exhibits a mono-stable periodic firing at the frequency $f \approx 23.5$ Hz for the considered parameters, the ring of such neurons (2) gets synchronized and fires at multiple frequencies ranging from approximately 10 Hz to 80 Hz and in numerous co-existing travelling waves [Fig. 7]. Such a multistability of travelling waves is already well pronounced for zero delay in the coupling [Fig. 7, blue diamonds], and it is significantly enhanced if a delay τ_j in coupling is introduced [Fig. 7, red circles for $\tau_j = 5$ ms and green squares for $\tau_j = 20$ ms]. Interestingly, as in the case of LC oscillators, in the FHN ensemble the delay does not change the frequency interval of possible synchronized dynamics. Even though the number of coexisting stable travelling waves increases for large delay, all of them fit into the same frequency range from 10 Hz to 80 Hz filling this interval more densely when the delay increases.

IV. VARIABILITY OF SPIKE PATTERNS IN NON-HOMOGENEOUS RINGS

In the case where the ring of coupled systems is not homogeneous, much more complicated structures are possible. As a result, the spike-encoding capability of such system increases drastically. In this section, we show in this section, that practically any stable spiking pattern can be created by an appropriate variation of the system's inhomogeneity. We consider the following types of inhomogeneities: variable delay times, variable coupling weights, and variable parameters of individual oscillators.

A. Firing patterns induced by inhomogeneous coupling delays

Varying time delays in coupling is possibly the most universal and simple way of creating different patterns. Let a general homogeneous network (3) with identical delays $\tau_j = \tau$ exhibit a stable periodic dynamics where neuron j fires at time moment t_j within one period. We refer to such a state as a reference pattern. It might for instance be an in-phase synchronization with $t_1 = t_2 = \cdots = t_n$ or any kind of stable travelling waves described in the previous section. Given a sequence of real numbers $\eta_1, \eta_2, \ldots, \eta_N$, the change of variables $\mathbf{y}_j(t) = \mathbf{x}_j(t - \eta_j)$ transforms this system to a system of the same form (3) but with inhomogeneous delays

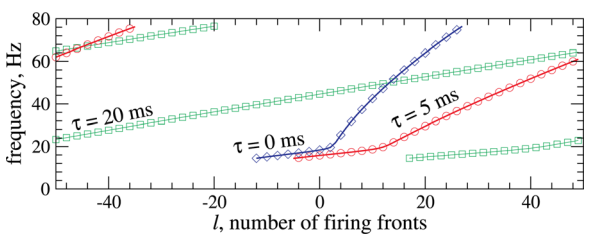

FIG. 7. (Color online) Multistability of travelling waves in the ring of $N = 100$ FHN neurons (2). The spiking frequency of the neurons exhibiting a stable travelling wave with l firing fronts propagating either in the direction of coupling ($l > 0$) or in the opposite direction ($l < 0$) is depicted versus l for delays $\tau_j = 0$ ms (blue diamonds), 5 ms (red circles), and 20 ms (green squares). The coupling weights $K_j = 2$.

$$\tau_j = \tau - \eta_{j+1} + \eta_j. \tag{9}$$

In the new system, neurons fire at times

$$\bar{t}_j = t_j + \eta_j, \quad j = 1, \ldots, N. \tag{10}$$

Thus, by choosing the delays appropriately, one can generate an almost arbitrary stable spiking pattern (10). Relation (9) provides an explicit expression for coupling delays, given any predefined sequence $\{\eta_j\}_{j=1}^N$. Note that for the in-phase reference pattern $t_1 = t_2 = \cdots = t_N$, the new spiking pattern $\{\bar{t}_j\}_{j=1}^N$ coincides with the sequence $\{\eta_j\}_{j=1}^N$, since t_j can be set to zero by a common time shift. The requirement for τ_j to be positive leads to the following limitation on the created pattern: the new inter-spike interval between two neighboring neurons $\bar{t}_{j+1} - \bar{t}_j$ cannot exceed the value $(t_{j+1} - t_j) + \tau$. This fact follows from the positiveness of τ_j and the following estimate

$$\bar{t}_{j+1} - \bar{t}_j = t_{j+1} - t_j + \tau - \tau_j < t_{j+1} - t_j + \tau.$$

In particular, if the reference pattern is the in-phase synchronized state, then $\bar{t}_{j+1} - \bar{t}_j < \tau$. Therefore, the coupling delay τ plays an important role by opening up the possibility for the emergence of nontrivial patterns. The larger the delay, the greater the possible spread of the firing times in the pattern.

The above arguments are actually independent of the particular form of the coupled individual systems and underlying dynamics. Moreover, similar arguments can be applied to an arbitrary coupling topology

$$\dot{\mathbf{x}}_j(t) = \mathbf{f}_j(\mathbf{x}_j(t)) + \mathbf{g}_j(\mathbf{x}_1(t - \tau), \ldots, \mathbf{x}_N(t - \tau)). \tag{11}$$

In this case, the above change of variables $\mathbf{y}_j(t) = \mathbf{x}_j(t - \eta_j)$ leads to the system with inhomogeneous delays

$$\dot{\mathbf{y}}_j(t) = \mathbf{f}_j(\mathbf{y}_j(t)) + \mathbf{g}_j(\mathbf{y}_1(t - \tau_{1j}), \ldots, \mathbf{y}_N(t - \tau_{Nj})), \tag{12}$$

where

$$\tau_{jp} = \tau - \eta_p + \eta_j$$

are the coupling delays from oscillator p to oscillator j. Indeed, by differentiating $\mathbf{y}_j(t)$, we obtain

$$\dot{\mathbf{y}}_j(t) = \dot{\mathbf{x}}_j(t - \eta_j) = \mathbf{f}_j(\mathbf{x}_j(t - \eta_j)) + \mathbf{g}_j(\mathbf{x}_1(t - \eta_j - \tau), \ldots, \mathbf{x}_N(t - \eta_j - \tau)).$$

Taking now into account that $\mathbf{x}_j(t - \eta_j) = \mathbf{y}_j(t)$ and $\mathbf{x}_p(t - \eta_j - \tau) = \mathbf{x}_p(t - \eta_p - (\tau - \eta_p + \eta_j)) = \mathbf{y}_p(t - \tau_{pj})$, we obtain Eq. (12). The firing times of Eqs. (11) and (12) are related again by the same simple expression (10). From this point of view, the ring of unidirectionally coupled systems plays the role of a minimal model with the minimal possible number of links N.

The above delay-induced patterns can be applied to any stable dynamics of FHN neurons (2). We illustrate this by a random pattern in Fig. 8. For this, we consider the FHN system with identical delays $\tau_j = 20$ ms, which possesses a stable in-phase synchronized firing pattern [Fig. 8(a), green

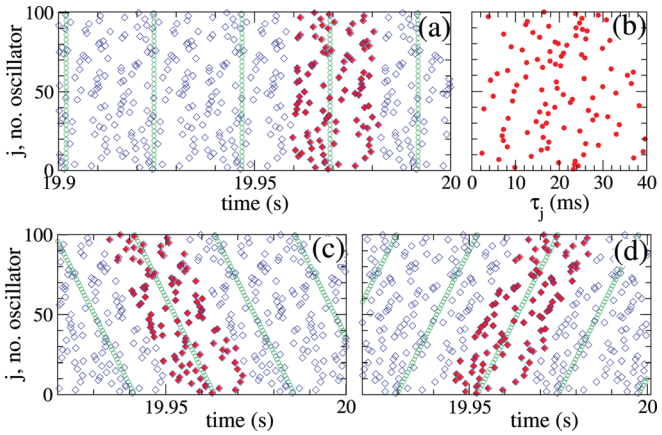

FIG. 8. (Color) Delay-induced firing patterns in the ensemble of $N=100$ FHN neurons (2). (a), (c), (d) Raster plots of the neuronal firing induced by inhomogeneous delays τ_j depicted in plot (b) for identical coupling weights $K_j=2$ and for different reference patterns depicted by green empty circles: (a) in-phase reference pattern, (c) and (d) travelling wave reference patterns with $l=1$ and $l=-1$ firing fronts, respectively, obtained for identical delays $\tau_j=20$ ms and coupling $K_j=2$. Blue empty diamonds indicate spike onsets obtained by numerical simulation of ensemble (2), and red filled diamonds depict the theoretically predicted pattern η_j adjusted to the firing times of the corresponding reference pattern, $\eta_j - Tlj/N$. To observe the above complex patterns the reference patterns were numerically continued by slowly approaching the predicted delays.

empty circles]. Then, we randomly choose a target firing pattern $\{\eta_j\}_{j=1}^N$, where the time shifts η_j are uniformly randomly distributed in the interval $[-20, 20]$ ms [Fig. 8(a), red filled diamonds], and compute the necessary coupling delays $\{\tau_j\}_{j=1}^N$ by Eq. (9). The corresponding distribution of the delays is shown in Fig. 8(b). After adjusting of the delay times to the newly computed values, the system shows a stable pattern [Fig. 8(a), blue empty diamonds], which periodically repeats the predicted targeted pattern $\{\eta_j\}$.

Note that the initial conditions leading to this pattern should be adjusted as well, since the system still possesses a high level of multistability [Fig. 7] and different initial conditions may lead to different patterns. For example, for the same delays as in Fig. 8(b) and for initial conditions resulting in the travelling waves with $l=\pm 1$ firing fronts for identical delays, we may obtain patterns [Figs. 8(c), 8(d), blue empty diamonds] which look somewhat different to that shown in Fig. 8(a). Nevertheless, we get a perfect overlap with the predefined pattern $\{\eta_j\}$ if it is adjusted by the corresponding time shifts t_j attributed to the given travelling wave, $\eta_j - Tlj/N$ [Figs. 8(c), 8(d), red filled diamonds]. This supports the simple relation (10) between the firing times of the reference pattern for the homogeneous ensemble and the firing patterns induced by distributed delays.

B. Firing patterns induced by inhomogeneous synaptic weights

We show that various firing patterns can equivalently be induced in neural networks by varying synaptic weights. To illustrate this, we first consider the LC oscillators (1) with homogeneous delays $\tau_j=\tau$.

Again, using the rotation symmetry of the system, one can look for periodic solutions of the form $z_j(t) = \rho_j e^{i\omega t + i\psi_j}$ with constant amplitudes ρ_j and phase shifts ψ_j. Substituting this ansatz into Eq. (1), we obtain the expressions for coupling weights K_j for a given phase pattern $\{\psi_j\}_{j=1}^N$

$$K_j = \frac{\rho_j}{\rho_{j+1}} \frac{\omega - \beta}{\sin(\psi_{j+1} - \psi_j - \omega\tau)}, \tag{13}$$

where

$$\rho_j = \sqrt{\alpha + (\omega - \beta)\cot(\psi_{j+1} - \psi_j - \omega\tau)} \tag{14}$$

are the corresponding amplitudes. Hence, for a given phase pattern $\{\psi_j\}_{j=1}^N$ and frequency ω, one can uniquely find coupling weights $\{K_j\}_{j=1}^N$ from Eqs. (13)–(14) leading to such a spatio-temporal pattern in ensemble (1). Since the stability of the predicted pattern is not known *a priori*, it is reasonable to choose ω as the frequency of a stable synchronized pattern in a corresponding homogeneous system with identical couplings $K_j=K$. In this case, $\omega-\beta=K\sin(\varphi_l-\omega\tau)$ (see Eq. (5)) and the coupling weights from Eq. (13) will lead to a stable pattern, at least for small modulations of the synchronous state.

We illustrate this approach on the ring of 100 LC oscillators (1) with $\tau_j=5$ ms and $K_j=2$. For these parameter values, there exists a stable in-phase synchronized pattern with frequency $\omega\approx 0.09$ s^{-1} (the time units in Eq. (1) are considered as milliseconds). We consider this state as a reference pattern [Fig. 9(a), green circles]. Then, we generate a random phase pattern $\{\psi_j\}$ [Fig. 9(a), red filled diamonds] and calculate the corresponding coupling weights K_j by Eqs. (13)–(14) [Fig. 9(b)]. The results of the numerical simulations of the LC ensemble (1) with the above inhomogeneous coupling weights are shown in Fig. 9(a) [blue empty diamonds], which perfectly agree with the theoretical prediction [Fig. 9(a), red filled diamonds].

In such a way, a broad spectrum of coupling-induced patterns can be generated in the ring of LC oscillators (1). We consider another, zig-zag pattern shown in Fig. 10(a) [red filled diamonds] and calculate the corresponding coupling weights using Eqs. (13)–(14) [Fig. 10(b)]. Such a distribution of the coupling weights induces a zig-zag pattern in

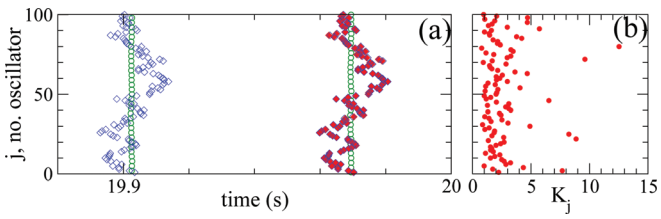

FIG. 9. (Color) Coupling-induced random pattern in a ring of $N=100$ LC oscillators (1) for identical delays $\tau_j=5$ ms. (a) Raster plot of the crossing of the Poincare section $\{x=0, y\geq 0\}$ by the oscillators' trajectories $\{z_j(t)=x_j(t)+iy_j(t)\}$ [blue empty diamonds]. The predefined pattern [red filled diamonds] is obtained by a uniform random distribution of the firing times $\{\eta_j\}$ in the interval $[-60$ ms, 60 ms] and smoothing them by a running average over 25 oscillators. The corresponding phase pattern $\{\psi_j\}$ is then calculated as $\psi_j=-2\pi\eta_j/T$, where T is the period of the reference in-phase synchronized pattern [green empty circles] of the homogeneous LC ensemble (1) for $K_j=2$ and $\tau_j=5$ ms. (b) The corresponding distribution of the coupling weights C_j obtained for the above predefined phase pattern $\{\psi_j\}$ from Eqs. (13)–(14). Parameters $\alpha=1$ and β_j are Gaussian distributed around $\beta=1$ with standard deviation 0.01.

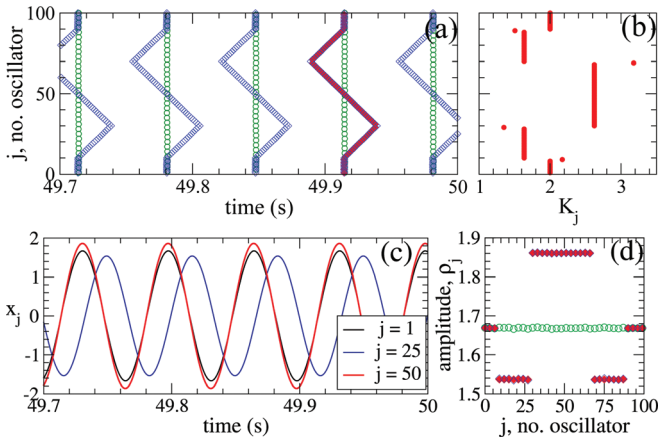

FIG. 10. (Color) (a) Coupling-induced zig-zag pattern in a ring of $N=100$ LC oscillators (1) for identical delays $\tau_j=5$ ms. (a) Raster plot of the return times of the oscillators to the Poincare section as in Fig. 9(a) with the same meaning of the colors. (b) The corresponding distribution of the coupling weights K_j. (c) Time courses of the trajectories $x_j(t)=\Re(z_j(t))$ for oscillators $j=1, 25$, and 50 as indicated in the legend. (d) Amplitudes $\rho_j=|z_j|$ of the oscillators corresponding to the patterns depicted in (a) with the same meaning of the colors. The other parameters as in Fig. 9.

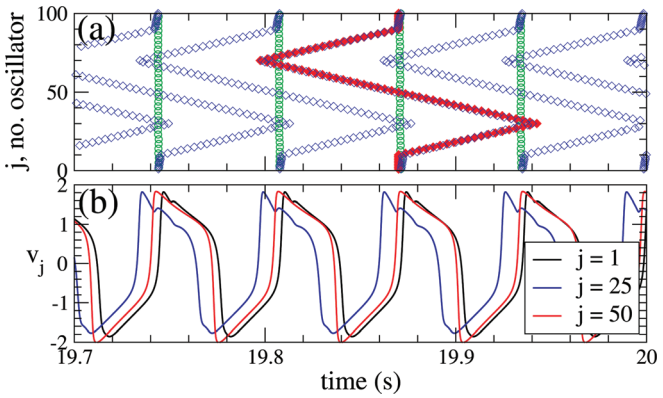

FIG. 11. (Color) (a) Coupling-induced zig-zag firing pattern in the ensemble of $N=100$ FHN neurons (2) for identical delays $\tau_j=5$ ms and inhomogeneous synaptic weights K_j from Fig. 10(b). (a) Raster plot of the neuronal firing where numerically simulated zig-zag pattern [blue empty diamonds] are compared with the theoretically predicted pattern scaled by a factor 2.9 [red filled diamonds] to fit the numerical results. Green circles depict in-phase synchronized reference pattern for identical $K_j=2$ and $\tau_j=5$ ms. (b) Time courses of the membrane potentials $v_j(t)$ for neurons $j=1, 25$, and 50 as indicated in the legend.

the LC ensemble, and, as before, the results of numerical simulations [Fig. 10(a), blue empty diamonds] perfectly agree with the theory [Fig. 10(a), red filled diamonds]. As follows from Eqs. (13)–(14), the inhomogeneous coupling influences the amplitudes ρ_j of the oscillators. Indeed, the oscillators' amplitudes of the zig-zag pattern are significantly changed [Figs. 10(c) and 10(d), blue empty diamonds] and strongly deviate from the uniform amplitudes of the in-phase synchronized reference pattern [Fig. 10(d), green circles]. Again, the theoretical prediction for the amplitudes [Fig. 10(d), red filled diamonds] nicely fits to the results of the numerical simulations.

In fact, formula (13) obtained for the LC oscillators (1) can effectively be used to generate coupling-induced patterns also in neuronal ensembles. We illustrate this on the FHN neurons (2). If the above coupling parameters K_j [Fig. 10(b)] are used for the excitatory coupled FHN neurons (2) as synaptic weights, the neuronal ensemble demonstrates qualitatively the same zig-zag pattern [Fig. 11(a), blue empty diamonds]. The results of numerical simulations can well be overlapped with the theoretically predefined pattern after its rescaling by some constant factor $t_j \to \text{const}\cdot t_j$ [Fig. 11(a), red filled diamonds]. This indicates that the expression (13) can empirically be used to generate coupling-induced patterns in neuronal ensembles. We note that the spike amplitudes are practically not affected by the inhomogeneous synaptic weights [Fig. 11(b)], which is in contrast to the LC oscillators [Fig. 10(c)], and only the resting states of the spiking dynamics are slightly influenced. Therefore, for the neuronal ensembles one may also utilize Eq. (13) where the amplitudes are ignored, i.e., letting $\rho_j \equiv 1$.

C. Cooperative effect of inhomogeneous delays and synaptic weights

The communication delays and synaptic weights, if adjusted simultaneously, may also have cooperative effects on the spatio-temporal firing patterns. We illustrate this phenomenon on a wave-like pattern [Fig. 12(a), blue empty diamonds] induced in the FHN neuronal ensemble (2) from the in-phase synchronized reference pattern [Fig. 12(a), green circles] by inhomogeneous synaptic weights K_j [Fig. 12(b)]. The latter are calculated by Eqs. (13)–(14) from the predefined phase pattern [Fig. 12(a), red filled diamonds].

In Fig. 12(a), the reference in-phase synchronized pattern is nearly completely overlapped by another in-phase synchronized state [Fig. 12(a), black triangles] which is obtained for FHN neurons when both synaptic weights

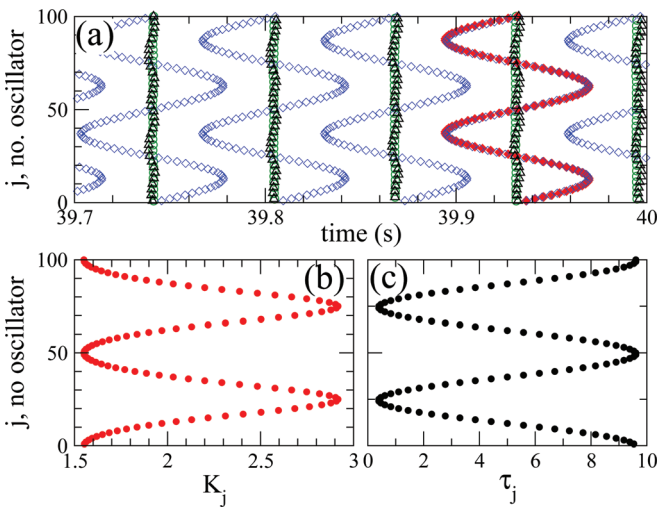

FIG. 12. (Color) Cooperative effect of inhomogeneous delays and synaptic weights on the spatio-temporal patterns in ensemble of $N=100$ FHN neurons (2). (a) Raster plot of the neuronal firing for in-phase synchronized reference patterns for identical delay $\tau_j=5$ ms and coupling $K_j=2$ [green circles]; wave-like pattern for inhomogeneous coupling K_j from plot (b) and identical delays $\tau_j=5$ ms [blue empty diamonds]; in-phase synchronized pattern for inhomogeneous coupling from plot (b) and delays from plot (c) [black triangles]. The theoretically predicted wave-like pattern for inhomogeneous coupling from plot (b) and $\tau_j=5$ ms is scaled by a factor of 2.9 [red filled diamonds] to fit the results of numerical simulations. (b) The corresponding synaptic weights K_j and (c) communication delays τ_j.

[Fig. 12(b)] and communication delays [Fig. 12(c)] are appropriately adjusted simultaneously. Therefore, an in-phase synchronization can for instance be obtained in either homogeneous neuronal ensemble for identical delays and synaptic weights [Fig. 12(a), green circles] or in a very inhomogeneous neuronal ensemble [Fig. 12(a), black triangles] for broadly distributed communication delays [Fig. 12(c)] and couplings [Fig. 12(b)]. The discussed cooperative effect of the adjustable delays and coupling strengths can even further increase the coding capability of the considered networks, where new patterns may be induced which are not accessible if only communication delays or only synaptic weights are varied.

D. Basins of attraction

Since the considered networks possess a great multistability of travelling waves, it is important to understand how accessible the delay- and coupling-induced patterns are. To address this issue, we calculate the basins of attraction of the corresponding complex spatio-temporal patterns. For the ring of LC oscillators (1), we consider a class of initial functions $\Gamma(t)$, $t \in [-\tau, 0]$, $\tau = \max_j \tau_j$, which can be parameterized by two parameters: temporal period T and spatial phase shift φ. In such a way, for given T and φ the initial function attains the form $\Gamma(t) = [\Gamma_1(t), \Gamma_2(t),\ldots,\Gamma_N(t)]^T$ with

$$\Gamma_j(t) = \gamma(t + \psi_j + \varphi j/N), \tag{15}$$

where the limit cycles $\gamma(t) = (\cos(2\pi t/T), \sin(2\pi t/T))$ have a unit amplitude and period T. The constant phase shifts ψ_j correspond to the investigated pattern and are considered as $\psi_j = 0$ for the homogeneous ensemble (in-phase synchronized initial state), the predefined phase shifts $\{\psi_j\}$ from Eqs. (13) and (14) for the coupling-induced patterns, and the corresponding phase shifts $\psi_j = -2\pi\eta_j/T$ for the delay-induced patterns, see Sec. IV A.

The homogeneous LC ensemble (1) for the considered parameters $K_j = 2$ and $\tau_j = 5$ ms (the time units in Eq. (1) are considered as milliseconds) has a stable in-phase synchronized state with the temporal period $T \approx 66.85$ ms. We thus investigate the ranges of the period $T \in [40, 100]$ms and the phase shift $\varphi \in [-4\pi, 4\pi]$ for the initial functions, which comprise the in-phase synchronized state ($l = 0$) and the travelling waves with $l = \pm 1$, ± 2 firing fronts. The basins of attraction of the above travelling waves for the homogeneous LC ensemble (1) are shaded in gray in Fig. 13(a) versus parameters (T, φ). One can notice that, for the considered range of parameters, there is a relatively weak dependence of the basin boundaries on the period T, whereas the spatial phase shift φ of the initial function plays a significant role in the selection of the desired travelling wave.

The basins of attraction of the delay-induced patterns are the same as for the homogeneous networks. This follows from the suggested change of the variables, see Sec. IV A, where the stability of the patterns is not affected. We also verified this for the inhomogeneous delays τ_j from Fig. 12(c). For the initial functions $\Gamma(t)$ from the gray region in Fig. 13(a) labeled "$l = 0$", the inhomogeneous LC ensemble

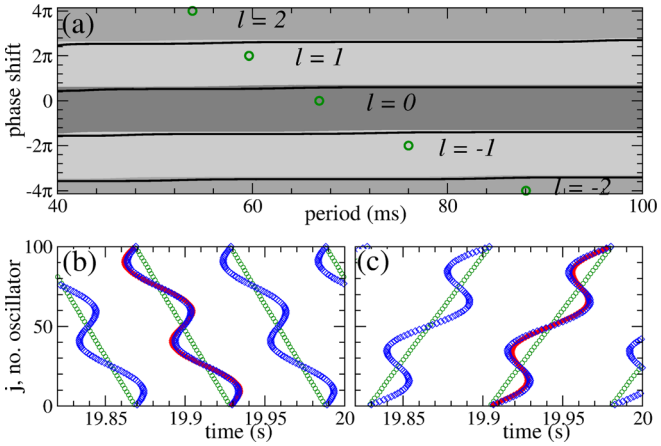

FIG. 13. (Color online) (a) Basins of attraction of the spatio-temporal patterns of the LC ensemble (1) for a two-parameter family of initial functions (15) versus initial period T and phase shift φ (see text for details). Gray regions show the basins of attraction of the travelling waves indicated by empty green circles with $l = 0$ (in-phase synchronization) and ± 1, ± 2 firing fronts for the homogeneous ensemble with $K_j = 2$ and $\tau_j = 5$ ms, and for delay-induced patterns for nonidentical delays τ_j from Fig. 12(c). The black solid curves depict basin boundaries for the coupling-induced S-shape patterns [Fig. 12(a)] for nonidentcal coupling weights K_j from Fig. 12(b). Two examples of the coupling-induced patterns realized for the initial conditions from the regions marked "$l = 1$" and "$l = -1$" are shown in plots (b) and (c) [blue empty diamonds], respectively. The corresponding predefined pattern [red filled diamonds] adjusted to the firing times of the reference pattern [green empty circles] is also shown. The other parameters as in Fig. 9.

(1) exhibits an S-shaped pattern inverted to that shown in Fig. 12(a) [red filled diamonds]. For the initial functions from other gray regions in Fig. 13(a), the skewed S-shaped patterns are realized, which are aligned along the corresponding travelling waves of the homogeneous LC ensemble with $l = \pm 1$, ± 2 firing fronts, respectively. Similarly as for the delay-induced random patterns illustrated for the FHN neurons in Figs. 8(c), 8(d), the skewed patterns can well be overlapped with the predefined pattern $\{\eta_j\}$ if the latter is adjusted to the firing times of the corresponding reference pattern, $\eta_j - Tlj/N$.

For the coupling-induced patterns of the inhomogeneous LC ensemble (1) the basins of attraction also have the same structure and nearly coincide with the basins of attraction for the travelling waves of the homogeneous ensemble. This is illustrated in Fig. 13(a) for the inhomogeneous coupling weights K_j taken from Fig. 12(b). The basin boundaries in this case are delineated by black solid curves. For the initial functions from the region labeled "$l = 0$" the S-shaped pattern [as in Fig. 12(a), red filled diamonds] is realized. For other initial functions, the S-shaped patterns get aligned along the corresponding reference patterns, i.e., travelling waves for the homogeneous ensemble with the corresponding number of the firing fronts l, see Figs. 13(b) and 13(c) [blue empty diamonds] for $l = 1$ and $l = -1$, respectively. Note that the shape of the coexisting skewed S-shaped patterns from Figs. 13(b) and 13(c) slightly deviates from that of the tilted predefined pattern even if the latter is adjusted to the firing times of the corresponding reference pattern, see the difference between red and blue diamonds in Figs. 13(b) and 13(c). This is in contrast to the delay-induced patterns and predicted by Eqs. (13) and (14). The reason for this

deviation is that the coupling weights K_j in Fig. 12(b) are calculated for the frequency ω of the in-phase synchronized reference pattern. If the oscillations occur at other frequencies, this will influence the shape of the realized patterns, as illustrated in Figs. 13(b) and 13(c).

As a result, we conclude that there exists a large region in the space of initial conditions, starting from which a desired stable delay- and/or coupling-induced pattern is realized in the inhomogeneous ensemble. The size of this region is similar to that of the corresponding reference pattern for the homogeneous network.

E. Firing patterns induced by inhomogeneous internal parameters of oscillators

The discussed spatio-temporal patterns can also be created by varying parameters of individual oscillators while keeping the communication delays and coupling strengths homogeneous. We demonstrate this effect on the ensemble of nonidentical LC oscillators

$$z_j' = (\alpha + i\beta)z_j - a_j^2 z_j|z_j|^2 + \mu z_{j+1}(t-\tau). \tag{16}$$

The change of variables

$$y_j(t) = a_j z_j(t) \tag{17}$$

with real constants a_j does not influence the phases of the oscillators, and, hence, the spatio-temporal phase patterns of both y_j and z_j solutions will be the same. In the new coordinates, system (16) attains the form of identical coupled oscillators

$$y_j' = (\alpha + i\beta)y_j - y_j|y_j|^2 + K_j y_{j+1}(t-\tau) \tag{18}$$

with inhomogeneous coupling weights

$$K_j = \frac{a_j}{a_{j+1}}\mu. \tag{19}$$

It is easy to see that by an appropriate adjustments of the nonlinearities a_j any possible coupling weight K_j can be obtained up to the restriction that the geometric mean of the coupling weights is fixed

$$(K_1 K_2 \cdots K_N)^{1/N} = \mu.$$

If we consider μ as another control parameter, then the coupling weights can attain arbitrary values by Eq. (18). Therefore, as follows from Sec. IV B, a variety of firing patterns can appear in such system, and, hence, in ensemble (16) of nonidentical oscillators with homogeneous couplings.

V. CONCLUSIONS

We showed that a practically arbitrary periodic spatio-temporal firing pattern can be produced by a feed-forward oscillatory neural loop if the communication delays or/and synaptic weights are appropriately adjusted with one restriction, namely, that each neuron fires only once per period of the pattern. The appropriate adjustment of the communication delays is directly reflected by the relative times of the neuronal firing irrespectively of the underlying neuronal dynamics. The variations of the synaptic weights, on the other hand, affect the phase differences between neurons, which might be important for the concept of phase delays as compared to the firing time differences explored in the auditory system.[66] A simultaneous variation of the communication delays and coupling weights can have a cooperative effect on the coordination of the neuronal firing which further extends the spectrum of possible firing patterns. We also show that a variety of spatio-temporal patterns can be induced by an appropriate adjustment of the internal parameters of the oscillators. An intriguing multitude of possible delay- and coupling-induced spatio-temporal firing patterns are illustrated on a minimal model of neural networks, and explicit formulas are presented which allow for a unique encoding of the patterns by communication delays and synaptic weights. Furthermore, as indicated in Sec. IV A, the presented approach can be extended to more complicated network topologies. In this paper, we illustrated our approach on the coupled limit-cycle oscillators and FitzHugh-Nagumo spiking neurons. Qualitatively the same results have also been obtained for the more complicated and realistic Hodgkin-Huxley model,[20] which indicates the robustness of the discussed phenomenon.

These findings contribute to the hypothesis of the temporal coding of information in neural networks by a precise timing of the neuronal firing. As mentioned in the Introduction, the signal propagation time latencies as well as synaptic weights can precisely be adapted in the brain, which may lead to a precise coordination of the neuronal firing, as we show in this paper.

ACKNOWLEDGMENTS

The authors acknowledge the support of the DFG Collaborative Research Center SFB910 under the project A3 (S.Y.), DFG Research Center MATHEON"Mathematics for key technologies" under the project D21 (S.Y. and P.P.), and Foundation for Polish Science, the START fellowship (P.P.).

[1]T. Heil, I. Fischer, W. Elsäßer, J. Mulet, and C. R. Mirasso, Phys. Rev. Lett. **86**, 795 (2001).
[2]R. Vicente, L. L. Gollo, C. R. Mirasso, I. Fischer, and G. Pipa, Proc Natl Acad Sci U.S.A **105**, 17157 (2008).
[3]M. Denker, M. Timme, M. Diesmann, F. Wolf, and T. Geisel, Phys. Rev. Lett. **92**, 074103 (2004).
[4]R. M. Memmesheimer and M. Timme, Physica D **224**, 182 (2006).
[5]B. Cessac, H. Paugam-Moisy, and T. Vieville, J. Physiol. **104**, 5 (2010).
[6]J. J. Hopfield, Nature **376**, 33 (1995).
[7]A. K. Engel, P. König, and W. Singer, Proc. Natl. Acad. Sci. U.S.A. **88**, 9136 (1991).
[8]H. Fujii, H. Ito, K. Aihara, N. Ichinose, and M. Tsukada, Neural Networks **9**, 1303 (1996).
[9]G. Buzsaki, Neuron **68**, 362 (2010).
[10]E. M. Izhikevich, Neural Computation **18**, 245 (2006).
[11]P. Tiesinga, J. M. Fellous, and T. J. Sejnowski, Nat. Rev. Neurosci. **9**, 97 (2008).
[12]N. Caporale and Y. Dan, Annu. Rev. Neurosci. **31**, 25 (2008).
[13]M. Salami, C. Itami, T. Tsumoto, and F. Kimura, Proc. Natl. Acad. Sci. U.S.A. **100**, 6174 (2003).
[14]W. Gerstner, R. Kempter, J. L. van Hemmen, and H. Wagner, Nature **383**, 76 (1996).
[15]W. Senn, M. Schneider, and B. Ruf, Neural Computation **14**, 583 (2002).

[16]C. W. Eurich, K. Pawelzik, U. Ernst, J. D. Cowan, and J. G. Milton, Phys. Rev. Lett. **82**, 1594 (1999).
[17]S. Boudkkazi, E. Carlier, N. Ankri, O. Caillard, P. Giraud, L. Fronzaroli-Molinieres, and D. Debanne, Neuron **56**, 1048 (2007).
[18]D. J. Bakkum, Z. C. Chao, and S. M. Potter, PLoS ONE **3**, e2088 (2008).
[19]A. Compston and A. Coles, Lancet **359**, 1221 (2002).
[20]O. V. Popovych, S. Yanchuk, and P. A. Tass, Phys. Rev. Lett. **107**, 228102 (2011).
[21]G. E. Alexander, M. R. Delong, and P. L. Strick, Annu. Rev. Neurosci. **9**, 357 (1986).
[22]E. Ahissar and D. Kleinfeld, Cereb. Cortex **13**, 53 (2003).
[23]H. Bergman and G. Deuschl, Mov. Disorders **17**, S28 (2002).
[24]N. Fogelson, D. Williams, M. Tijssen, G. van Bruggen, H. Speelman, and P. Brown, Cereb. Cortex **16**, 64 (2006).
[25]C. Hammond, R. Ammari, B. Bioulac, and L. Garcia, Mov. Disord. **23**, 2111 (2008).
[26]M. Golubitsky, I. Stewart, P. Buono, and J. Collins, Nature **401**, 693 (1999).
[27]A. Kumar, S. Rotter, and A. Aertsen, Nat. Rev. Neurosci. **11**, 615 (2010).
[28]G. B. Ermentrout and D. Kleinfeld, Neuron **29**, 33 (2001).
[29]I. Waller and R. Kapral, Phys. Rev. A **30**, 2047 (1984).
[30]H. Daido, Phys. Rev. Lett. **78**, 1683 (1997).
[31]P. C. Bressloff, S. Coombes, and B. de Souza, Phys. Rev. Lett. **79**, 2791 (1997).
[32]I. P. Marino, V. Pérez-Mu nuzuri, V. Pérez-Villar, E. Sánchez, and M. A. Matías, Phys. D **128**, 224 (1999).
[33]S. Yanchuk, Y. Maistrenko, and E. Mosekilde, Math. Comput. Simul **54**, 491 (2001).
[34]Y. Zhang, G. Hu, and H. A. Cerdeira, Phys. Rev. E **64**, 037203 (2001).
[35]J. G. Restrepo, E. Ott, and B. R. Hunt, Phys. Rev. Lett. **93**, 114101 (2004).
[36]D. M. Abrams and S. H. Strogatz, Phys. Rev. Lett. **93**, 174102 (2004).
[37]R. Dodla, A. Sen, and G. L. Johnston, Phys. Rev. E **69**, 056217 (2004).
[38]G. V. der Sande, M. C. Soriano, I. Fischer, and C. R. Mirasso, Phys. Rev. E **77**, 055202 (2008).
[39]S. Yanchuk and M. Wolfrum, Phys. Rev. E **77**, 026212 (2008).
[40]W. Zou and M. Zhan, SIAM J. Appl. Dyn. Syst. **8**, 1324 (2009).
[41]M. Bonnin, Physica D **238**, 77 (2009).
[42]P. Perlikowski, S. Yanchuk, O. V. Popovych, and P. A. Tass, Phys. Rev. E **82**, 036208 (2010).
[43]P. Perlikowski, S. Yanchuk, M. Wolfrum, A. Stefanski, P. Mosiolek, and T. Kapitaniak, Chaos **20**, 013111 (2010).
[44]F. Pasemann, Neural Networks **8**, 421 (1995).
[45]S. J. Guo and L. H. Huang, Acta Math. Sin. English Ser. **23**, 799 (2007).
[46]M. A. Matías and J. Güémez, Phys. Rev. Lett. **81**, 4124 (1998).
[47]X. L. Deng and H. B. Huang, Phys. Rev. E **65**, 055202 (2002).
[48]K. Pakdaman, C. P. Malta, C. Grotta-Ragazzo, O. Arino, and J.-F. Vibert, Phys. Rev. E **55**, 3234 (1997).
[49]Y. Horikawa and H. Kitajima, Physica D **238**, 216 (2009).
[50]P. Baldi and A. Atia, IEEE Trans. Neural Netw. **5**, 1045 (1994).
[51]X. Pei, L. Wilkens, and F. Moss, Phys. Rev. Lett. **77**, 4679 (1996).
[52]A. Neiman, L. Schimansky-Geier, A. Cornell-Bell, and F. Moss, Phys. Rev. Lett. **83**, 4896 (1999).
[53]Y. Kuramoto, *Chemical Oscillations, Waves, and Turbulence* (Springer, Berlin, 1984).
[54]R. FitzHugh, Biophys. J. **1**, 445 (1961).
[55]J. Nagumo, S. Arimoto, and S. Yoshizawa, Proc. IRE **50**, 2061 (1962).
[56]W. Gerstner and W. M. Kistler, *Spiking Neuron Models: Single Neurons, Populations, Plasticity* (Cambridge University Press, Cambridge, 2002).
[57]E. M. Izhikevich, *Dynamical Systems in Neuroscience: The Geometry of Excitability and Bursting* (MIT, Cambridge, MA, 2005).
[58]D. Golomb and J. Rinzel, Phys. Rev. E **48**, 4810 (1993).
[59]D. Terman, J. E. Rubin, A. C. Yew, and C. J. Wilson, J. Neurosci. **22**, 2963 (2002).
[60]M. Golubitsky and D. G. Schaeffer, *Singularities and Groups in Bifurcation Theory. Volume I*, Applied Mathematical Sciences Vol. 51 (Springer-Verlag, New-York, 1985).
[61]M. Golubitsky, I. Stewart, and D. G. Schaeffer, *Singularities and Groups in Bifurcation Theory. Volume II*, Applied Mathematical Sciences Vol. 69 (Springer-Verlag, New-York, 1988).
[62]S. Yanchuk and P. Perlikowski, Phys. Rev. E **79**, 046221 (2009).
[63]J. Foss, A. Longtin, B. Mensour, and J. Milton, Phys. Rev. Lett. **76**, 708 (1996).
[64]J. Foss, F. Moss, and J. Milton, Phys. Rev. E **55**, 4536 (1997).
[65]J. Foss and J. Milton, J Neurophysiol **84**, 975 (2000).
[66]C. Leibold and J. L. van Hemmen, Phys. Rev. Lett. **94**, 168102 (2005).